Applied Surface Science 669 (2024) 160478

Contents lists available at ScienceDirect

Applied Surface Science

journal homepage: www.elsevier.com/locate/apsusc

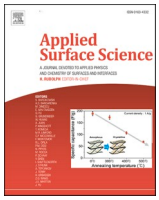

Full Length Article

Fabrication of monolayer h-BN/LaB_6 heterostructure thin film with low work function and high chemical stability

Katsumi Nagaoka [a,*], Takashi Aizawa [a], Shun-ichiro Ohmi [b]

[a] Research Center for Materials Nano-architectonics, National Institute for Materials Science, Tsukuba 305-0044, Japan
[b] Department of Electrical and Electronic Engineering, Tokyo Institute of Technology, Yokohama 226-8502, Japan

ARTICLE INFO

Keywords:
Heterostructure thin film
Surface precipitation
Lanthanum hexaboride (LaB_6)
Low work function
monolayer hexagonal boron nitride (h-BN)

ABSTRACT

To expand the applications of low work function materials, high chemical stability is necessary to prevent the surface from unfavorable reactions. We developed a 20-nm-thick lanthanum hexaboride (LaB_6) thin film covered by a monolayer hexagonal boron nitride (h-BN), which exhibits not only low work function but also high chemical stability. Results demonstrated that the h-BN/LaB_6 heterostructure can be formed by vacuum annealing a nitrogen-doped LaB_6 thin film. The formation process was investigated using Auger electron spectroscopy (AES), high-resolution electron energy loss spectroscopy (HREELS), and X-ray absorption near edge structure (XANES) spectroscopy. We have elucidated that the doped nitrogen atoms and boron atoms in the film thermally diffuse into the surface during annealing, thereby forming the monolayer h-BN on the surface. Work function was measured using scanning tunneling microscopy (STM). From a practical perspective, chemical stability was evaluated with a heating temperature necessary for restoring the low work function state after air exposure. The work function was comparable to that of the clean LaB_6(100) surface. Moreover, it recovered at a much lower temperature than the cleaning temperature of the LaB_6(100) surface. We anticipate that this material development will facilitate implementation of the low work function material.

1. Introduction

Work function is an important property for electron materials because it governs electron transfer characteristics at interfaces with vacuum or semiconductor materials. Particularly low work function is quite useful for electron devices of various kinds to achieve their higher performance.

One promising application of a low work function material is to use it for an electrode material in semiconductor devices. In this application, room temperature operation is supposed. One advantage of using a low work function material is that unintended Schottky effects are suppressed. A Schottky barrier is often formed at the interface between a metal and a semiconductor [1]. Such an unintended Schottky barrier between the semiconductor device and the external circuitry adversely affects the device performance and reliability. One solution to avoid this problem is to use a low work function material for the electrode to realize ohmic contact at the interface [2]. At present, however, low work function materials are hardly used as the electrode material for semiconductor devices. A main problem is that a conventional low work function material reacts with ambient gases during the device fabrication process, and then would have been no longer a low work function material [3]. Therefore, a low work function material accompanying high chemical stability is awaiting, which can withstand the fabrication process.

Lanthanum hexaboride (LaB_6), with a work function of 2.3 eV [3–6] is one of the low work function materials in practical use. However, the application field is still limited. The primary application of the LaB_6 is thermionic electron cathode [7–9]. Since it works at a temperature of 1200 °C or higher in vacuum, the surface is prevented from oxidation, maintaining its low work function for a long time. Even though thermionic electron emission can occur even below 1200 °C, the operating temperature of 1200 °C is necessary to maintain the clean surface [10]. Therefore, if it had high chemical stability, it could be operated at lower temperatures. In the lower temperature operation, thermal deterioration is suppressed, and the lifetime of the thermionic source can be expected to be extended. Low work function materials with high chemical stability would expand the application field and improve the performance of devices.

As a candidate, monolayer hexagonal-boron nitride (h-BN) / LaB_6 heterostructure film is proposed [11]. First, the work function of this

* Corresponding author.
E-mail address: NAGAOKA.Katsumi@nims.go.jp (K. Nagaoka).

https://doi.org/10.1016/j.apsusc.2024.160478
Received 8 March 2024; Received in revised form 24 May 2024; Accepted 4 June 2024
Available online 6 June 2024

system is expected to be as low as that of LaB_6. Fig. 1 presents a potential diagram around the surface of the monolayer h-BN/LaB_6 heterostructure thin film. In this system, the charge transfer is expected to be negligibly small because of the large band-gap of h-BN. Then the energy levels of the monolayer h-BN film and the substrate are aligned at the vacuum level (E_{vac}) rather than the Fermi level (E_F). Therefore, the work function of the system (Φ_{hetero}) is given by that of the substrate (Φ_{sub}) [12]. In addition, unfavorable reactions can be suppressed because the surface is covered with an inert film, i.e., the monolayer h-BN film [13–18]. Indeed, h-BN coated surfaces was suggested to be promising candidates for anti-corrosion applications, and h-BN nanosheet coatings using pulsed laser deposition techniques with h-BN targets have also been reported [19]. Consequently, chemical stability would be improved without increasing the work function.

A recent report has described lowering of the work function of single-crystal LaB_6(1 0 0) coated with a monolayer h-BN film prepared using wet-transfer method [20]. However, practical use of heterostructures is still awaiting increased ease of producing structures with various substrates and with various heterostructure sizes and shapes.

We have developed a 20-nm-thick thin film with monolayer h-BN/LaB_6 heterostructure on the surface. The heterostructure can be formed by vacuum annealing of a nitrogen (N) doped LaB_6 thin film [21–23], which can be fabricated on various substrates using radio-frequency (RF) sputtering deposition. Results showed that 20 nm thickness is sufficient to produce the desired function. The developed monolayer h-BN/LaB_6 heterostructure thin film is a material combining the low work function and high chemical stability, which are usually mutually exclusive. We expect the monolayer h-BN/LaB_6 heterostructure thin film to be seized upon as an opportunity for extending the applications of low work function thin films and improving the performance of devices using low work function materials.

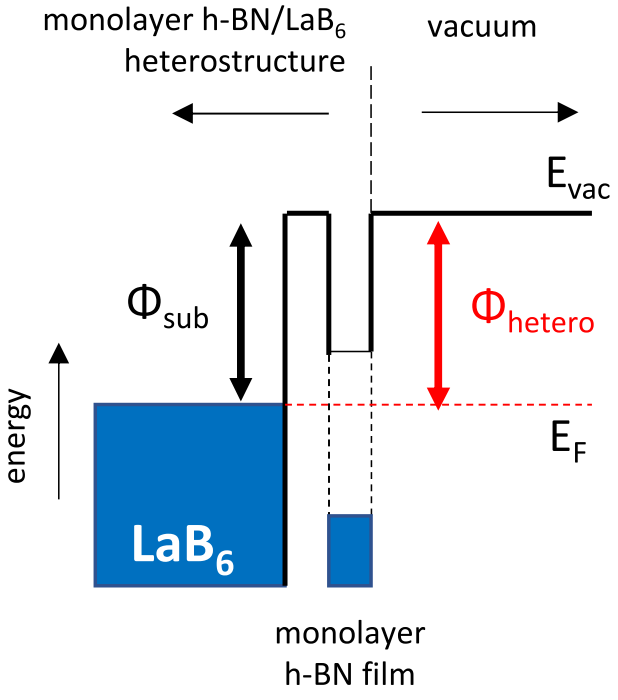

Fig. 1. Potential diagram around the surface of the monolayer h-BN/LaB_6 heterostructure thin film. E_{vac} and E_F respectively denote the vacuum level and Fermi level. Φ_{hetero} and Φ_{sub} respectively correspond to the work function of the system and that of the substrate.

2. Materials and methods

2.1. Sample preparation

The starting sample was a N-doped LaB_6 thin film deposited on SiO_2 or LaB_6(1 0 0) substrates [21]. The film thickness was 20 nm. The N-dope LaB_6 film was prepared using RF sputtering deposition, where the LaB_6 target containing 0.4 wt% nitrogen was used. This deposition process was identical to the initial process used to fabricate top-contact/back-gate organic field-effect transistors in earlier studies [24–29]. The N-doped LaB_6 thin film fabricated using this method is polycrystalline but highly oriented in the ⟨1 0 0⟩ direction [21]. After the nitrogen-doped LaB_6 thin film was deposited, the sample was removed from the deposition system into the ambient atmosphere and stored. All measurements were performed in ultra-high vacuum (UHV) systems. Depending on the system used for experimentation, the annealing method was chosen from electron bombardment, heater contact, and electrical heating. The temperature was measured using an optical pyrometer.

2.2. Experiment methods

Experiments were conducted to elucidate the segregation process of the monolayer h-BN on the LaB_6 film surface and to demonstrate the coexistence of the low work function and high chemical stability. The formation process was analyzed using Auger electron spectroscopy (AES), high-resolution electron energy loss spectroscopy (HREELS), and X-ray absorption near edge structure (XANES) spectroscopy, whereas the work function and the chemical stability were evaluated using scanning tunneling microscopy (STM).

For elucidating the formation process of the monolayer h-BN/LaB_6 heterostructure, annealing-temperature dependent surface analysis was performed on the N-doped LaB_6 thin film deposited on a LaB_6(0 0 1) single-crystal substrate. First, AES and HREELS measurements were conducted for identifying the surface composition and the structure. All measurements were conducted at room temperature.

The sample was annealed in UHV of the AES system at a desired temperature for 300 s by electron bombardment on the backside. We applied AES to the prepared sample *in situ* using a cylindrical mirror analyzer. The 15 keV electron beam was impinged on the sample for excitation at approximately 70° from the surface normal. Measurements were taken in the *dN/dE* mode using a lock-in amplifier. The elemental composition of the surface was estimated qualitatively from the AES. The sample of interest was moved in UHV to the HREELS system through a transfer tube.

The HREELS measurements were taken using a HREEL spectrometer (Delta 0.5; SPECS GmbH) operated with 1.5–2 meV resolution to obtain a reasonable signal-to-noise ratio. Because the sample was polycrystalline, HREEL spectra were taken only in the specular condition, where the incidence and detection angles were fixed at 75° from the surface normal. The loss peaks in the spectrum are attributed to surface phonon energies, which enable identification of the surface species or the bonding nature.

As a complementary method for identifying the material structure, The XANES measurement was performed. The XANES is a specific structure observed with X-ray absorption spectroscopy. When an atom absorbs X-rays, a core-level electron of the atom can be removed leaving behind a hole. The core hole can be filled by an outer shell electron, whereby the electron transitioning to the lower energy level loses an amount of energy equal to the difference in energy of the initial and final orbitals. The transition yields emission of fluorescent X-rays or Auger electrons with the characteristic energy equal to the difference in the orbital energies.

For acquiring a XANES spectrum, the method detecting the fluorescent X-rays is called the fluorescence yield method (TFY), and the method measuring Auger electrons and the secondary electrons induced by them is called the electron yield method (TEY) [30,31]. These two

methods give similar spectra since they are triggered with the identical X-ray absorption process mentioned above. But the main difference is recognized to be the information depth resulting from the difference in the escape depth of X-ray fluorescence and Auger electrons; it is on the order of a few micrometers for fluorescent X-rays, whereas it is on the order of several nanometers for Auger electrons. Accordingly, the TFY method provides bulk information, whereas the TEY method gives surface-sensitive data.

The XANES measurements were carried out at the BL5S1, hard X-ray XAFS beamline, at Aichi Synchrotron Radiation Center 21 (AichiSR; Aichi Science and Technology Foundation, Aichi, Japan). XANES spectra reveal the electronic configuration of valence states, chemical bonding properties, and local coordination of specific atoms. It can serve as a fingerprinting technique for material identification. For this study, the nitrogen K-edge XANES spectra were examined; h-BN powder was also used as a reference sample. Measurements were taken simultaneously in both TFY and TEY modes [30,31]. For the XANES measurements, the sample was heated by contact with a heat source. Measurements were taken at room temperature. A typical data reduction procedure (e.g., background removal, or normalization) was conducted using Athena version 0.9.26.

As the next step, coexistence of the low work function and the high chemical stability on the monolayer h-BN/LaB_6 heterostructure thin film was attempted to prove as described hereinafter. Because the fabricated film was polycrystalline, the work function was expected to vary at the cluster scale. Therefore, we decided to measure local work functions using STM sequentially and to visualize spatial distributions of the local work functions as a work function map [32,33].

For evaluating the work function using STM, it is first necessary to measure the effective potential barrier height for the tunneling electrons, which is called "apparent barrier heigh", and then the work function is calculated from the apparent barrier height. Using the tunneling current; I, the apparent barrier height; Φ_A, is derived from the logarithmic change-rate of tunneling current with respect to the tip–sample separation z at a certain bias voltage [23,34–36], and written as

$$\Phi_A(eV) = 0.952\left[\frac{d(\ln I(nA))}{dz(\text{Å})}\right]^2$$

Thus, the apparent barrier height is measured by applying a sinusoidal voltage on the z-axis piezo to modulate the tip-surface distance, and then detecting a response in the tunneling current at the frequency using a lock-in amplifier.

On the other hand, based on the Wentzel-Kramers-Brillouin (WKB) approximation, the apparent barrier height is supposed to be equivalent to the average potential height formed within the tunnelling gap. Therefore, the apparent barrier height can be written in terms of the sample work function (Φ_{sample}) as

$$\Phi_A \approx \{\Phi_{sample} + (\Phi_{tip} + V_s)\}/2 \quad (2)$$

where V_s is the sample bias voltage (<0 V), and Φ_{tip} is the work function of the STM tip. Using this formula, the work function can be calculated from the experimentally obtained apparent barrier height.

The STM measurements were taken at 77 K using a PtIr tip with an Omicron LT-STM system operated by RHK electronics. A topographic image was obtained in constant current mode. Simultaneously, work function mapping was acquired from the response of tunneling current to the change of tunnel gap distance during scanning. The modulation of the tip-to-surface distance was 1.0 Å with a frequency of 1.0 kHz. The modulation amplitude in ln I was measured using a lock-in amplifier.

For this study, chemical stability was evaluated with the heating temperature necessary for recovering the low work function state. The N-doped LaB_6 film was annealed in UHV at 900 °C to make a low-work-function surface. Subsequently, it was exposed to atmospheric-pressure air for 300 s, returned to UHV, and heated for surface recovery at a certain trial temperature. Then the work function mapping was examined to ascertain whether the low work function state was restored uniformly, or not.

3. Results

3.1. AES measurements

Fig. 2 presents the AES spectra of the N-doped LaB_6 film for different annealing temperatures. A series of AES measurements was started with the as-deposited (as-depo) sample surface. The AES measurements were repeated while increasing the annealing temperature in 50 °C increments. On the as-depo sample, no N-Auger peak was detected. However, the La NVV- and B KVV- Auger peaks were confirmed respectively at 82 and 180 eV [37], accompanied by the contaminant C KVV (274 eV) and O KVV (520 eV) peaks. When the annealing temperature reached 800 °C, a nitrogen KVV peak appeared at 384 eV [38] in addition to those of La and B. The peak intensities of the nitrogen increased with the annealing temperature, although the peak disappeared when the annealing temperature reached 1200 °C.

3.2. HREELS measurements

To identify the chemical species of the nitrogen compound formed on the film surface, we measured HREEL spectra for the annealing temperatures of 700–1200 °C. This range includes the temperatures at which the nitrogen peak was detected in the AES spectra.

In the obtained spectra (Fig. 3), three characteristic peaks were observed at 101, 175, and 186 meV. These peaks are associated with the nitrogen compounds formed on the surface. The peak assignments were made based on comparison with the spectra presented in an earlier report [39]. Actually, 101, 175, and 186 meV can be assigned respectively $TO_{\perp}$, $TO_{//}$, and LO phonon modes of h-BN, and are almost equal to the corresponding vibrational energies of the monolayer h-BN formed

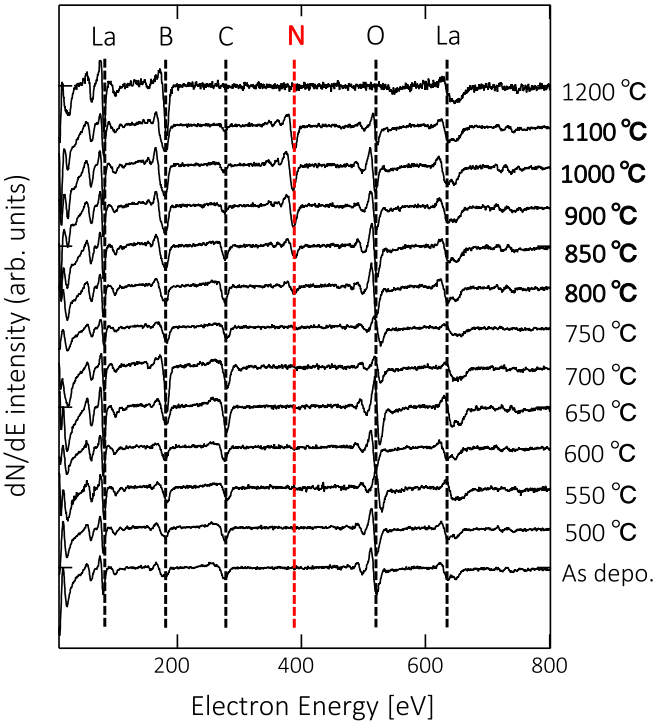

Fig. 2. Auger electron spectra of the N-doped LaB_6 film for different annealing temperatures. Annealing temperatures are shown on the right side of each spectrum. Dashed lines correspond to the peak positions for each element.

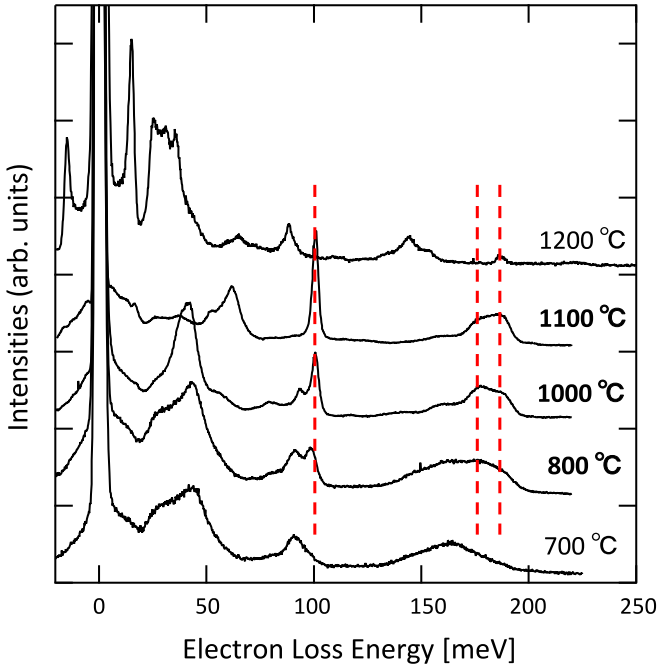

Fig. 3. HREEL spectra of the N-doped LaB_6 film for different annealing temperatures. Annealing temperatures are shown on the right side of each spectrum. Dashed lines correspond to the characteristic peak positions for the samples of which the nitrogen peaks were detected in the AES spectra (Fig. 2).

on Ni, Pd, and Pt (1 1 1), which indicates that the h-BN thin film was formed on the LaB_6 surface. In particular, the phonon energies measured in our system are close to those of the incommensurate h-BN/Ni(1 1 1), rather than those of the commensurate h-BN/Ni(1 1 1), and are larger by only 2–3 meV. This result seems convincing, because all phonons in the incommensurate system, such as h-BN/Pd(1 1 1) or h-BN/Pt(1 1 1), exhibited higher energies than those in the commensurate system, such as h-BN/Ni(1 1 1), by 3–8 meV, which trend was confirmed to be followed in our system as well.

Since the surface phonon energy is associated with a lattice vibration of the surface, each material has its own unique values. However, the phonon dispersion of h-BN is very similar to that of graphene. This is because they have the identical crystal structure and the comparable lattice constants, and the average atomic weights of B and N are almost equal to that of C. For distinguishing between the two, the energy dispersion of the surface phonons should have been measured. But this was not possible on our system because it was polycrystalline. Instead, the AES measurements showed that B and N were dominant on the surface, so the formation of graphene was excluded.

3.3. XANES measurements

As a complementary method for identifying the h-BN/ LaB_6 heterostructure formation other than HREELS, XANES measurements were taken. For our measurements, sample annealing was conducted at 900 °C by contacting the heater onto the back side of the sample holder plate. The XANES spectra were measured around the nitrogen K-edge in TEY and TFY modes simultaneously, which are respectively surface-sensitive and bulk-sensitive.

The XANES spectra of the annealed N-doped LaB_6 film sample are presented in Fig. 4. As a reference, those of the h-BN powder are shown. For quantitative comparison, the theoretical XANES spectra of the N K-edges of h-BN and lanthanum nitride (LaN), which were obtained from the Materials Project database [40] and calculated with an energy resolution of 1.5 eV, are also presented. In common to the TEY and TFY spectra of the annealed N-doped LaB_6 film, there exist two peaks at 417

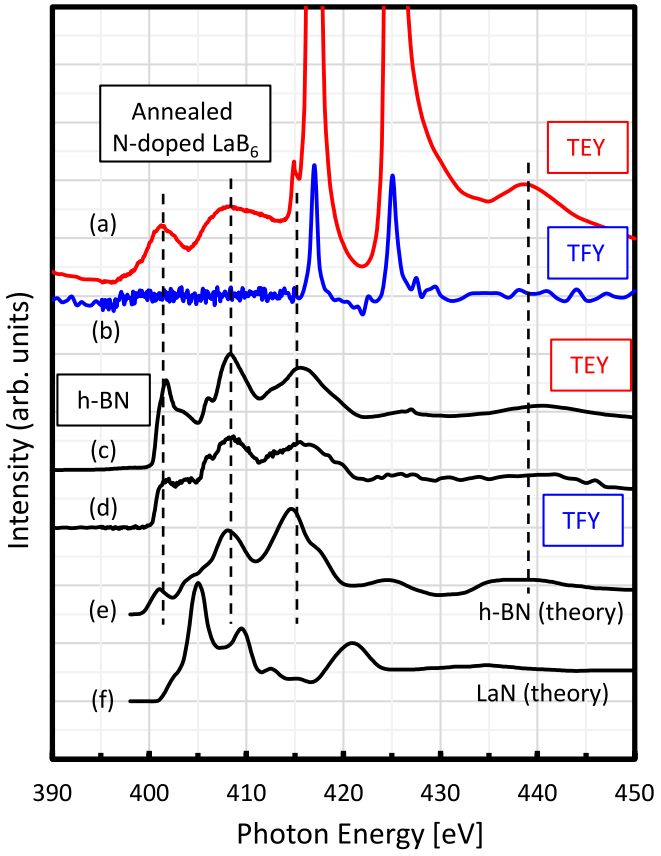

Fig. 4. (a)(b) XANES spectra of the 900 °C-annealed N-doped LaB_6 film measured around the nitrogen K-edge in TEY and TFY modes. (c)(d) For comparison, XANES spectra of the h-BN powder measured around the nitrogen K-edge in TEY and TFY modes. Dashed lines correspond to the characteristic peak positions of h-BN. (e)(f) Theoretical XANES spectra around the nitrogen K-edge of h-BN and LaN, obtained from the Materials Project database [40].

and 425 eV. These peaks are attributed to the half-energy of the X-ray absorption energy of the La-M edge [41,42]. However, a significant difference can be seen as follows. In the surface-sensitive TEY mode, absorption peaks appeared at 401, 408, and 439 eV, whereas these peaks were not detected in the TFY mode which mainly provides bulk information. These peaks are assigned as characteristic of h-BN, because the identical features were found in the spectrum of h-BN powder and theoretical spectrum, as well as in previous study [43]. Comparing between the two modes, the main difference is the information depth, which is a few nanometers for TEY mode and a few micrometers for TFY mode, depending on the escape depth of Auger electrons and X-ray fluorescence, respectively. Therefore, the XANES data clearly indicate that the h-BN existed only on the surface but not in the bulk, which supports that annealing the N-doped LaB_6 thin film makes a monolayer h-BN/LaB_6 heterostructure grow on the surface.

3.4. STM measurements

We next demonstrated the coexistence of the low work function and high chemical stability on the monolayer h-BN /LaB_6 heterostructure thin film. The STM measurements were started with the trial heating temperature set at 450 °C after air exposure. Fig. 5a shows a typical topographic STM image after the trial heating. The simultaneously obtained work function mapping is also presented in Fig. 5b, in which the higher brightness area corresponds to the higher work function area. Fig. 5c corresponds to the work function profile along the dotted line in (b). The dashed line corresponds to 2.3 eV, which is the ideal work function of the clean LaB_6(1 0 0) surface [44]. At any point, the local

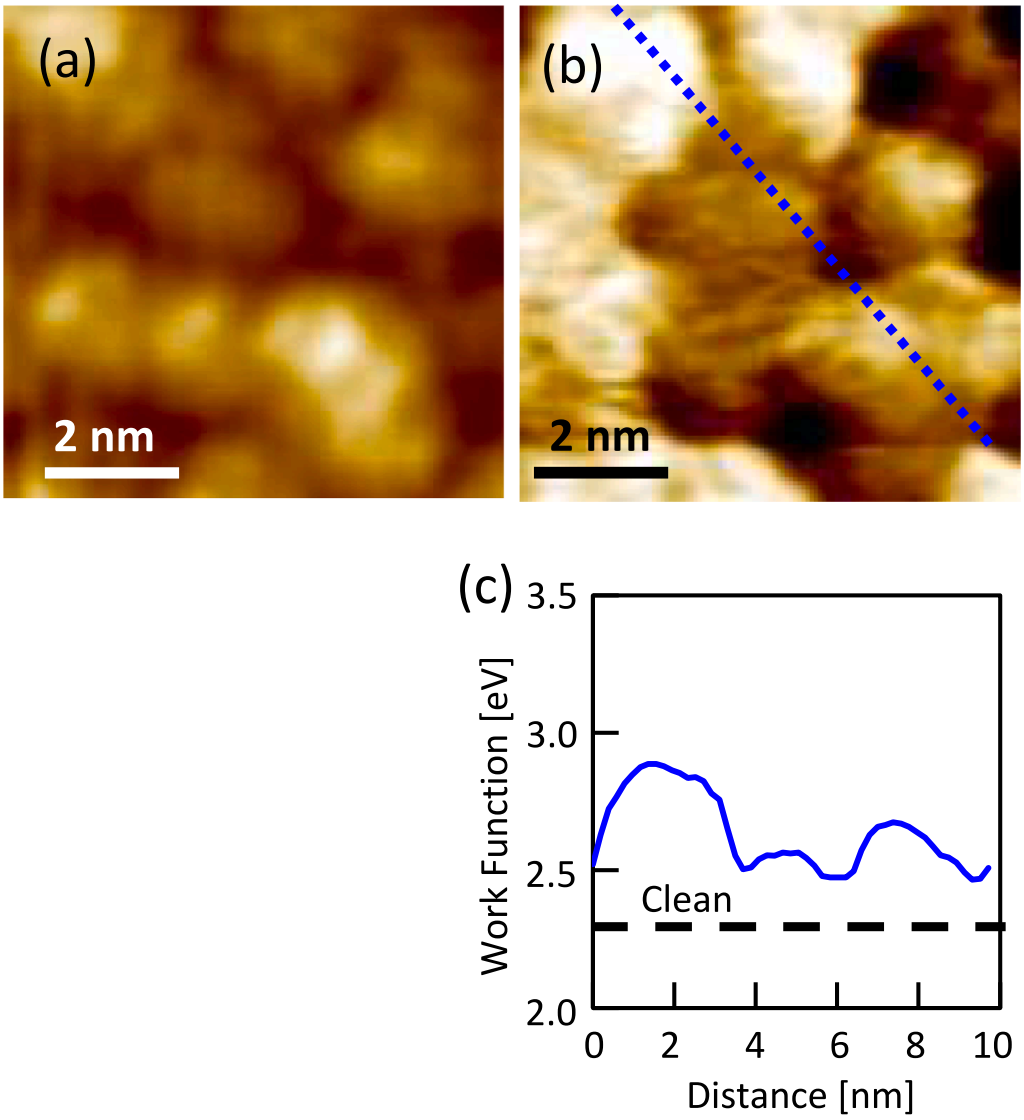

Fig. 5. (a) Typical topographic STM image of the monolayer h-BN LaB_6 heterostructure thin film after trial heating at 450 °C, $I = 0.5$nA at Vs = -3.50 V, 8 nm × 8 nm, and (b) the simultaneously obtained work function mapping. (c) Work function profile along the dotted line in (b). The dashed line corresponds to the work function of the clean LaB_6(1 0 0) surface, 2.3 eV.

work functions were higher than 2.3 eV. The values varied widely from cluster to cluster. This finding means that heating at 450 °C remained insufficient to restore the low work function state.

Then, the trial heating temperature was increased to 550 °C. The STM measurements were conducted in the same manner. Fig. 6a and 6b respectively show a topographic STM image and the work function mapping. Fig. 6c corresponds to the work function profile along the dashed line in Fig. 6(b). The work function mapping shows that the work function of 2.35 eV has been achieved over a wide range. Therefore, we have ascertained the heating temperature necessary to restore the low work function state to be 550 °C.

The obtained recovery temperature, 550 °C, was much lower than the temperature required for cleaning the LaB_6(1 0 0) surface, 1300 °C [44,45]. In fact, it is comparable to those for cleaning the highly oriented pyrolytic graphite (HOPG) [46] and the monolayer h-BN film grown on the transition metals [12]. This result indicates that the monolayer h-BN film improved the chemical stability of the LaB_6 surface without increasing the work function of the system.

However, the local work function appears to be lower than 2.35 eV in some spots. These areas of low function are apparently artifacts specific to this measurement method [47], which is seen on non-horizontal planes such as gap regions between clusters and explained as below.

For obtaining the work function mapping, the tip-to-surface distance is modulated in the z direction in scanning, and then the apparent barrier height is derived from the dI/dz signal intensity acquired with a lock-in amplifier at each point. Therefore, for measuring the work function value, the tip oscillation direction is critical and should be perpendicular to the surface. Indeed, when the oscillation direction deviates θ from the vertical direction, the effective displacement from the surface varies in proportion to cos θ geometrically, and then the signal intensity is attenuated proportionally. Consequently, the obtained value for the apparent barrier height decreases according to $(\cos\theta)^2$ from the formula (1).

For the above reason, when the work function mapping is performed on an inclined surface, the lower value is derived as the work function than the actual value is. Such an underestimation of the work function is often noticeable near grain boundaries due to the geometrical problem.

4. Discussion

First, the monolayer h-BN/LaB_6 heterostructure formation process is discussed. The AES measurements did not detect the doped nitrogen in

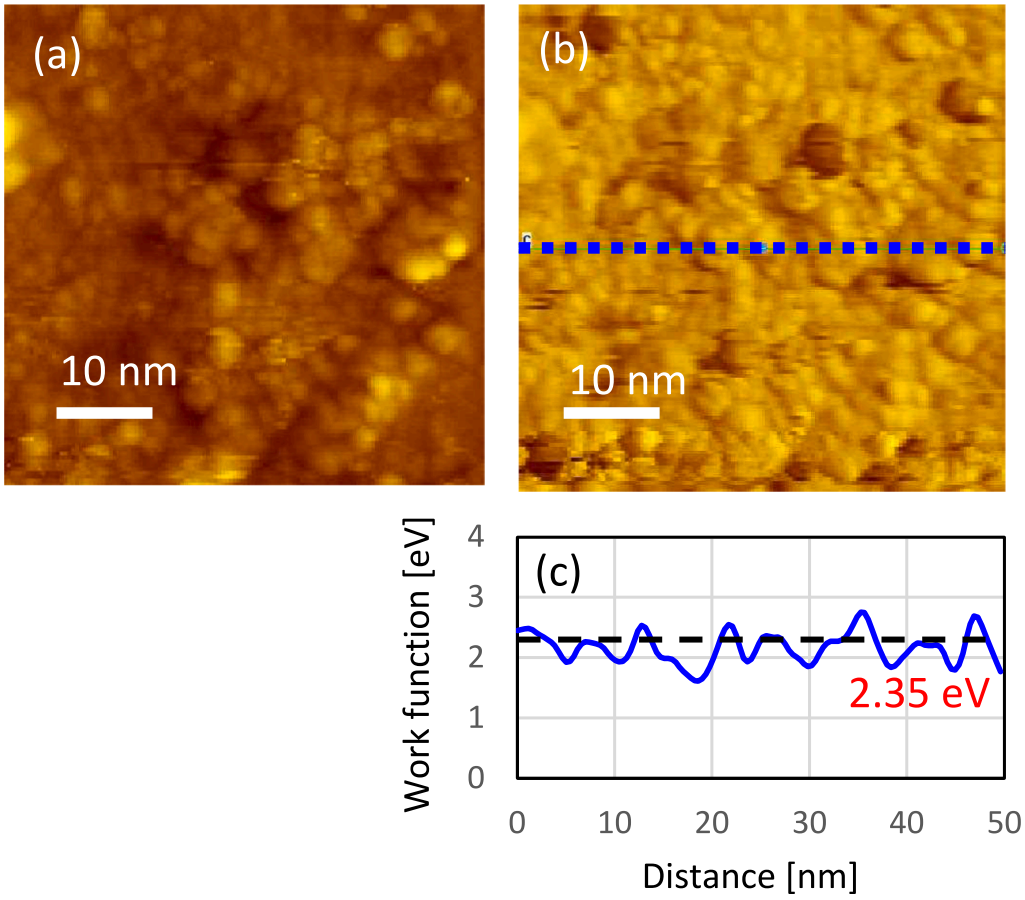

Fig. 6. (a) Typical topographic STM image of the monolayer h-BN LaB_6 heterostructure thin film after trial heating at 550 °C, $I = 0.5$nA at $Vs = -3.50$ V, 50 nm × 50 nm, and (b) the simultaneously obtained work function mapping. (c) Work function profile along the dotted line in (b).

the as-depo state, but detected it after annealing at appropriate temperatures. The HREELS and XANES measurements revealed that the nitrogen forms a h-BN film on the surface.

Based on these experimentally obtained results, we propose the growth model portrayed in Fig. 7. In the as-depo state, the doped nitrogen atoms might be weakly bound around the grain boundaries in the polycrystalline LaB_6 film. However, when the film is annealed at temperatures higher than 800 °C, thermal diffusion of the doped nitrogen atom would occur. Then the nitrogen atoms react with surrounding boron atoms of the LaB_6 to form a h-BN film and to aggregate on the surface.

The driving force for diffusion into the surface is probably a decrease in the surface free energy due to the h-BN formation on the surface. The formation energy of the h-BN is 1.318 eV/atom obtained from the Materials Project database [40]. This value is considered to be enough large for surface precipitation to occur [48]. In fact, surface precipitation of h-BN has been confirmed on the surface of BN-doped stainless steel [49]. Besides, on the (1 1 1) surface of a carbon (C)-doped Ni single crystal, multilayer and monolayer graphite films were reported to be formed at high temperatures in UHV [50]. This phenomenon was also explained with the surface free energy, depending on the graphite formation on the surface.

As a competitive process against the h-BN formation, that of LaN, whose formation energy is 1.575 eV/atom [40], could be possible. But the theoretical N K-edge XANES spectrum of the LaN [40] did not match the XANES spectrum we obtained (Fig. 4). Therefore, the formation of LaN in this system seems unlikely.

The thickness of the grown h-BN film is expected to be a single layer

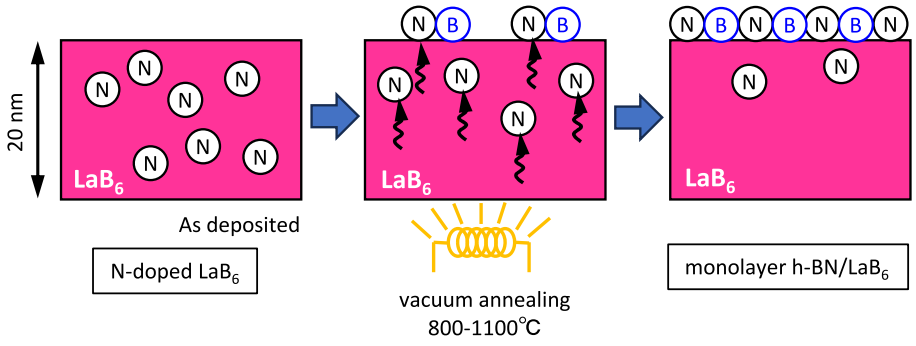

Fig. 7. Schematic diagram of the formation process of a monolayer h-BN/LaB_6 heterostructure.

because of the following reasons: in the HREEL spectrum for the annealing temperature at 1100 °C, the dominant features were associated with the h-BN film, presuming that almost the entire surface was covered with the h-BN film. However, in AES measurements, which have lower surface sensitivity than the HREELS measurements [51,52], La atoms were also detected in addition to B and N atoms, even on an identical sample. For XANES measurements, the absorption peaks of the h-BN appeared only in the surface sensitive TEY mode, but they were not detected in the TFY mode. By contrast, the absorption peak of La was observed in both modes. Considering the surface sensitivities [53] of the measuring methods we used, the formed h-BN film thickness can be inferred as that of one layer.

In order to quantitatively prove that the formed h-BN is monolayer thick, we have focused on the nitrogen content in the nitrogen-doped LaB_6 thin film prepared by the RF sputtering deposition. Since the nitrogen content in the LaB_6 target used in this study was 0.4 wt%, the nitrogen content in the fabricated thin film would be at most 0.4 wt%. Based on this value, area density of the nitrogen was estimated to be 16.2 atom/nm for the 20 nm-thick film. This nitrogen amount corresponds to that of the h-BN thin film for 0.9 layer, which means that the prepared nitrogen-doped LaB_6 film contained insufficient amount of nitrogen to form the multilayer h-BN film. In fact, once the h-BN was sublimated by annealing at 1200 °C, nitrogen was depleted, and even after annealing the sample at the temperature appropriate for forming the h-BN thin films, no nitrogen was detected by AES. In light of the discussion presented above, it seems reasonable to assign that the thickness of the grown h-BN film is a single layer.

We attempted to obtain an atomic resolution STM image on the surface of the monolayer h-BN/LaB_6 heterostructure film, but so far we have not obtained it. The plausible reason is that the crystallinity was not high enough, since the substrate was a polycrystalline film prepared by the RF sputtering deposition. In the STM observation of the monolayer h-BN film, the substrate directly influences the acquiring image. In fact, it is reported that moiré patterns are induced on incommensurate system, such as monolayer h-BN/Pd(1 1 1) [54] and monolayer h-BN/Pt (1 1 1) [55]. In our system, the substrate for the h-BN film was a polycrystalline LaB_6 film prepared by RF sputtering deposition. The topographic image shows that the grain size was on the order of several nanometers, suggesting that the crystallinity of the underlying LaB_6 thin film did not seem high enough. Therefore, we have concluded that obtaining the atomic resolution was hard for present conditions.

In order to obtain atomic resolution STM images of the h-BN thin film in our system, it is absolutely necessary to improve the crystallinity of the underlying LaB_6 thin film. As future work, we are considering optimizing the conditions for the deposition and annealing of the nitrogen-doped LaB_6 thin film.

In the AES measurements, oxygen was detected even after h-BN formation on the surface. The work function of LaB_6 is known to be sensitive to oxygen adsorption [3]. But we obtained the work function of 2.35 eV after the h-BN layer formation, suggesting that the LaB_6 surface is free from oxygen under the h-BN layer. Currently, we infer the reason as the following: Because our sample was not a single crystal but a polycrystalline thin film prepared using RF sputtering deposition, the oxygen in the residual gas during deposition was probably involved into the film. An earlier report suggests that the involved oxygen affects the film crystallinity [19]. After annealing for the h-BN formation, oxygen might diffuse into the grain boundaries and remain there.

Currently, it is hard to quantitatively evaluate the defect density, because the prepared film was polycrystalline with grains of several nm. Impurities such as oxygen detected by AES are thought to have been involved from residual gas during RF sputtering deposition. However, in the later application stage with the monolayer h-BN/LaB_6 heterostructure thin film, improving the film quality is crucial. So, we believe that it is essential to improve the deposition environment and to optimize the film formation conditions for establishing the method for fabricating the high-quality film.

In this study, a unique growth method has been developed for an atomic layered film on a deposited thin film. To date, growth of atomic layered films has been investigated mainly on bulk single crystal surfaces. Aside from thermal precipitation of the graphite films on the C-doped Ni(1 1 1) surface [46], chemical vapor deposition (CVD) methods for h-BN [56] and graphene [57] on transition metal (1 1 1) surfaces and pyrolysis method for graphene on C-terminated SiC(0001) surface [58,59] are known. By the method we developed, monolayer h-BN growth is achieved on a thin film prepared by RF sputtering deposition via *ex-situ* vacuum annealing. To our knowledge, the monolayer h-BN/LaB_6 heterostructure thin film is the first example that atomic layered film was grown on the surface of a deposited thin film via *ex-situ* annealing. Since the heterostructure can be prepared from a 20 nm-thick thin film fabricated using RF sputter deposition, this method has practical advantageous features, such as high degrees of freedom in substrate selection and shape, and high scalability. We anticipate that this material development facilitates implementation of the low work function material, and that it contributes to solving problems related to interfacial electron transport, and consequently to expanding the application field and improving the performance of various electronic devices.

5. Conclusion

A 20-nm-thick thin film with a monolayer h-BN/LaB_6 heterostructure on its surface was developed. The heterostructure film was found to be obtained by annealing the N-doped LaB_6 thin film prepared by the RF sputtering deposition. The heterostructure formation process was investigated using AES, HREELS, and XANES spectroscopy. The results elucidated that the doped nitrogen atoms thermally diffused by annealing react with boron atoms of the LaB_6, and form the h-BN film on the surface. Additionally, the thickness of the h-BN film grown on the surface was revealed to be one monolayer.

The monolayer h-BN/LaB_6 heterostructure thin film was demonstrated to have both low work function and high chemical stability, which are usually mutually exclusive. In this study, the work function was measured using STM, and the chemical stability was evaluated with the heating temperature necessary for restoring the low work function state after exposure to air. Consequently, the work function of the heterostructure thin film was found to be 2.35 eV, which is comparable to that of the clean LaB_6(1 0 0) surface, whereas the recovery temperature was found to be 550 °C, which is considerably lower than the cleaning temperature of the ordinary LaB_6 surface. This finding constitutes experimentally obtained evidence demonstrating that the heterostructure improves chemical stability while maintaining the low work function.

Because the monolayer h-BN/LaB_6 heterostructure thin film is grown on the surface of the deposited thin film via *ex-situ* annealing, a high degree of freedom in shape and high scalability are also achieved. Therefore, the monolayer h-BN/LaB_6 heterostructure thin film we developed can be expected to expand the application field and improve the performance of various electronic devices.

CRediT authorship contribution statement

Katsumi Nagaoka: Writing – review & editing, Writing – original draft, Investigation, Data curation, Conceptualization. **Takashi Aizawa:** Writing – review & editing, Investigation. **Shun-ichiro Ohmi:** Writing – review & editing, Resources.

Declaration of competing interest

The authors declare that they have no known competing financial interests or personal relationships that could have appeared to influence the work reported in this paper.

Data availability

Data will be made available on request.

Acknowledgements

The authors would like to thank Dr. T. Goto of Tokyo Electron Technology Solutions Ltd. and Mr. K. Takahashi of Sumitomo Osaka Cement for their useful discussion and support of this research. This work was partly supported by JSPS KAKENHI (Grant Nos. 17K05066, 19H00758, and 15K13969) and the NIMS-DENKA Centre of Excellence for Next Generation Materials.

References

[1] R.T. Tung, The physics and chemistry of the Schottky barrier height, Appl. Phys. Rev. 1 (2014) 011304, https://doi.org/10.1063/1.4858400.
[2] S.M. Sze, Semiconductor Devices: Physics and Technology, Second Ed., John Wiley & Sons, Inc, 2002.
[3] R. Nishitani, C. Oshima, M. Aono, T. Tanaka, S. Kawai, H. Iwasaki, S. Nakamura, Oxygen adsorption on the LaB_6(100), (110) and (111) surfaces, Surf. Sci. 115 (1982) 48–60, https://doi.org/10.1016/0039-6028(82)90660-4.
[4] J.M. Lafferty, Boride Cathodes, J. Appl. Phys. 22 (1951) 299–309, https://doi.org/10.1063/1.1699946.
[5] H. Ahmed, A.N. Broers, Lanthanum hexaboride electron emitter, J. Appl. Phys. 43 (1972) 2185, https://doi.org/10.1063/1.1661472.
[6] M. Trenary, Surface science studies of metal hexaborides, Sci. Technol. Adv. Mater. 13 (2012) 023002, https://doi.org/10.1088/1468-6996/13/2/023002.
[7] A.N. Broers, Some experimental and estimated characteristics of the lanthanum hexaboride rod cathode electron gun, J. Phys. E 2 (1969) 273, https://doi.org/10.1088/0022-3735/2/3/310.
[8] A.N. Broers, High-resolution thermionic cathode scanning transmission electron microscope, Appl. Phys. Lett. 22 (1973) 610, https://doi.org/10.1063/1.1654527.
[9] H. Ahmed, E. Munro, Optimization of the performance of high-brightness electron guns, J. Vac. Sci. Technol. 10 (1973) 972, https://doi.org/10.1116/1.1318529.
[10] M. Futamoto, M. Nakazawa, K. Usami, S. Hosoki, U. Kawabe, Thermionic emission properties of a single-crystal LaB_6 cathode, J. Appl. Phys. 51 (1980) 3869–3876, https://doi.org/10.1063/1.328132.
[11] K. Nagaoka, T. Aizawa, S. Ohmi, Laminate, electron source and electronic device contacting laminate, and production method and cleaning method for laminate, World Intellectual Property Organization (WIPO), Patent Cooperation Treaty (PCT), WO 2023/048139 A1.
[12] A. Nagashima, N. Tejima, Y. Gamou, T. Kawai, C. Oshima, Electronic structure of monolayer hexagonal boron nitride physisorbed on metal surfaces, Phys. Rev. Latt. 75 (1995) 3918, https://doi.org/10.1103/PhysRevLett.75.3918.
[13] A.K. Geim, I.V. Grigorieva, Van der Waals heterostructures, Nature 499 (2013) 419–425, https://doi.org/10.1038/nature12385.
[14] K.S. Novoselov, A. Mishchenko, A. Carvalho, A.H. Castro Neto, 2D materials and van der Waals heterostructures, Science 353 (2016) aac9439, https://doi.org/10.1126/science.aac9439.
[15] H. Yamaguchi, J. Granstrom, W. Nie, H. Sojoudi, T. Fujita, D. Voiry, M. Chen, G. Gupta, A.D. Mohite, S. Graham, M. Chhowalla, Reduced graphene oxide thin films as ultra barriers for organic electronics, Adv. Energy Mater. 4 (2014) 1300986, https://doi.org/10.1002/aenm.201300986.
[16] F. Liu, N.A. Moody, K.L. Jensen, V. Pavlenko, C.W.N. Villarrubia, A.D. Mohite, G. Gupta, Single layer graphene protective gas barrier for copper photocathodes, Appl. Phys. Lett. 110 (2017) 041607, https://doi.org/10.1063/1.4974738.
[17] C.S. Rout, P.D. Joshi, R.V. Kashid, D.S. Joag, M.A. More, A.J. Simbeck, M. Washington, S.K. Nayak, D.J. Late, Superior field emission properties of layered WS_2-RGO nanocomposites, Sci. Rep. 3 (2013) 3282, https://doi.org/10.1038/srep03282.
[18] U.V. Patil, A.S. Pawbake, L.G.B. Machuno, R.V. Gelamo, S.R. Jadkar, C.S. Rout, D. J. Late, Effect of plasma treatment on multilayer graphene: X-ray photoelectron spectroscopy, surface morphology investigations and work function measurements, RSC Adv. 6 (2016) 48843–48850, https://doi.org/10.1039/C6RA03046G.
[19] A. Kumar, G. Malik, M.K. Pandey, R. Chandra, R.S. Mulik, Corrosion behavior of pulse laser deposited 2D nanostructured coating prepared by self-made h-BN target in salinity environment, Ceram. Int. 47 (2021) 12537–12546, https://doi.org/10.1016/j.ceramint.2021.01.111.
[20] H. Yamaguchi, R. Yusa, G. Wang, M.T. Pettes, F. Liu, Y. Tsuda, A. Yoshigoe, T. Abukawa, N.A. Moody, S. Ogawa, Work function lowering of LaB_6 by monolayer hexagonal boron nitride coating for improved photo- and thermionic-cathodes, Appl. Phys. Lett. 122 (2023) 141901, https://doi.org/10.1063/5.0142591.
[21] H. Ishii, K. Takahashi, T. Goto, S. Sugawa, T. Ohmi, Low work function LaB_6 thin films prepared by nitrogen doped LaB_6 target sputtering, ECS Trans. 66 (2015) 23, https://doi.org/10.1149/06641.0023ecst.
[22] K. Nagaoka, W. Hayami, S. Ohmi, Scanning tunneling spectroscopy study of 20 nm-thick nitrogen-doped lanthanum hexaboride thin film, Vacuum 170 (2019) 108973, https://doi.org/10.1016/j.vacuum.2019.108973.
[23] K. Nagaoka, S. Ohmi, Bias-voltage-dependent measurement of apparent barrier height on low-work function thin film, J. Vac. Sci. Technol. B 38 (2020) 062801, https://doi.org/10.1116/6.0000436.
[24] Y. Maeda, S. Ohmi, T. Goto, T. Ohmi, High quality pentacene film formation on N-doped LaB_6 donor layer, IEICE Trans. Electron. E99-C (2016) 535, https://doi.org/10.1587/transele.E99.C.535.
[25] Y. Maeda, S. Ohmi, Steep subthreshold swing of pentacene-based organic field-effect transistor with nitrogen-doped LaB_6 interfacial layer, Jpn. J. Appl. Phys. 56 (2017), 04CL06 0.7567/JJAP.56.04CL06.
[26] Y. Maeda, S. Ohmi, T. Goto, T. Ohmi, Effect of Nitrogen-Doped LaB_6 Interfacial Layer on Device Characteristics of Pentacene-Based OFET, IEICE Trans. Electron. E100-C (2017) 463, https://doi.org/10.1587/transele.E100.C.463.
[27] Y. Maeda, M. Hiroki, S. Ohmi, Investigation of pentacene growth on SiO_2 gate insulator after photolithography for nitrogen-doped LaB_6 bottom-contact electrode formation, Jpn. J. Appl. Phys. 57 (2018) 04FL13, https://doi.org/10.7567/JJAP.57.04FL13.
[28] Y. Maeda, K.E. Park, M. Hiroki, Y. Komatsu, S. Ohmi, Pentacene-based depletion load pMOS inverter realized by threshold voltage control utilizing nitrogen-doped LaB_6 interfacial layer, Jpn. J. Appl. Phys. 58 (2019) 060909, https://doi.org/10.7567/1347-4065/ab21a3.
[29] K.E. Park, S. Ohmi, The influence of high-temperature sputtering on the N-Doped LaB_6 thin film formation utilizing RF sputtering, IEICE Trans. Electron. E103-C (2020) 293–298, https://doi.org/10.1587/transele.2019FUP0004.
[30] W. Gudat, C. Kunz, Close similarity between photoelectric yield and photoabsorption spectra in the Soft-X-Ray range, Phys. Rev. Lett. 29 (1972) 169, https://doi.org/10.1103/PhysRevLett.29.169.
[31] J. Jaklevic, J.A. Kirby, M.P. Klein, A.S. Robertson, G.S. Brown, P. Eisenberger, Fluorescence detection of EXAFS: sensitivity enhancement for dilute species and thin films, Solid State Commun. 23 (1977) 679, https://doi.org/10.1016/0038-1098(77)90548-8.
[32] Y. Hasegawa, J.F. Jia, K. Inoue, A. Sakai, T. Sakurai, Elemental contrast of local work function studied by scanning tunneling microscopy, Surf. Sci. 386 (1997) 328, https://doi.org/10.1016/S0039-6028(97)00332-4.
[33] J.F. Jia, K. Inoue, Y. Hasegawa, W.S. Yang, T. Sakurai, Variation of the local work function at steps on metal surfaces studied with STM, Phy. Rev. B. 58 (1998) 1193, https://doi.org/10.1103/PhysRevB.58.1193.
[34] G. Binnig, H. Rohrer, Ch. Gerber, E. Weibel, Tunneling through a controllable vacuum gap, Appl. Phys. Lett. 40 (1982) 178, https://doi.org/10.1063/1.92999.
[35] N.D. Lang, Apparent barrier height in scanning tunneling microscopy, Phys. Rev. B 37 (1988) 10395, https://doi.org/10.1103/PhysRevB.37.10395.
[36] G. Binnig, H. Rohrer, Scanning tunneling microscopy, Surf. Sci. 126 (1983) 236, https://doi.org/10.1016/0039-6028(83)90716-1.
[37] L.W. Swanson, T. Dickinson, Single-crystal work-function and evaporation measurements of LaB_6, Appl. Phys. Lett. 28 (1976) 578–580, https://doi.org/10.1063/1.88597.
[38] K.P. Loh, I. Sakaguchi, M. Nishitani-Gamo, T. Taniguchi, T. Ando, Surface structure of single-crystal cubic boron nitride (111) studied by LEED, EELS, and AES, Phys. Rev. B 56 (1997) R12791(R), https://doi.org/10.1103/PhysRevB.56.R12791.
[39] E. Rokuta, Y. Hasegawa, K. Suzuki, Y. Gamou, C. Oshima, A. Nagashima, Phonon dispersion of an epitaxial monolayer film of hexagonal boron nitride on Ni(111), Phys. Rev. Lett. 79 (1997) 4609, https://doi.org/10.1103/PhysRevLett.79.4609.
[40] A. Jain, S.P. Ong, G. Hautier, W. Chen, W.D. Richards, S. Dacek, S. Cholia, D. Gunter, D. Skinner, G. Ceder, K.A. Persson, Commentary: the materials project: a materials genome approach to accelerating materials innovation, APL Mater. 1 (2013) 011002, https://doi.org/10.1063/1.4812323.
[41] J.A. Bearden, A.F. Burr, Reevaluation of X-Ray atomic energy levels, Rev. Mod. Phys. 39 (1967) 125, https://doi.org/10.1103/RevModPhys.39.125.
[42] C.L. Perkins, M. Trenary, T. Tanaka, S. Otani, X-ray photoelectron spectroscopy investigation of the initial oxygen adsorption sites on the LaB_6(100) surface, Surf. Sci. 423 (1999) L222–L228, https://doi.org/10.1016/S0039-6028(98)00936-4.
[43] J.B. MacNaughton, A. Moewes, R.G. Wilks, X.T. Zhou, T.K. Sham, T. Taniguchi, K. Watanabe, C.Y. Chan, W.J. Zhang, I. Bello, S.T. Lee, H. Hofsäss, Electronic structure of boron nitride single crystals and films, Phys. Rev. B 72 (2005) 195113, https://doi.org/10.1103/PhysRevB.72.195113.
[44] R. Nishitani, M. Aono, T. Tanaka, C. Oshima, S. Kawai, H. Iwasaki, S. Nakamura, Surface structures and work functions of the LaB_6 (100), (110) and (111) clean surfaces, Surf. Sci. 93 (1980) 535–549, https://doi.org/10.1016/0039-6028(80)90281-2.
[45] P.R. Davis, S.A. Chambers, A study of oxygen interaction with a LaB_6(100) single crystal surface, Appl. Surf. Sci. 8 (1981) 197–205, https://doi.org/10.1016/0378-5963(81)90015-5.
[46] W. Xie, L.T. Weng, K.M. Ng, C.K. Chan, C.-M. Chan, Clean graphene surface through high temperature annealing, Carbon 94 (2015) 740–748, https://doi.org/10.1016/j.carbon.2015.07.046.
[47] S. Kurokawa, M. Yuasa, A. Sakai, Y. Hasegawa, Barrier-height imaging of oxygen-adsorbed Si(111) 7×7 surfaces, Jpn. J. Appl. Phys. 36 (1997) 3860, https://doi.org/10.1143/JJAP.36.3860.
[48] K. Nii, Surface characterization and performance of surface-treated materials(I); Surface segregation, surface precipitation and surface oxidation, Corros. Eng. (jpn.) 31 (1982) 664, https://doi.org/10.3323/jcorr1974.31.10_664.
[49] K. Yoshihara, M. Tosa, K. Nii, Surface precipitation of boron nitride on the surface of type 304 stainless steels doped with nitrogen, boron, and cerium, J. Vac. Sci. Technol. A 3 (1985) 1804–1808, https://doi.org/10.1116/1.573383.
[50] M. Eizenberg, J.M. Blakely, Carbon monolayer phase condensation on Ni(111), Surf. Sci. 82 (1979) 228, https://doi.org/10.1016/0039-6028(79)90330-3.
[51] J.H. Wandass, J.A. Gardella Jr., Vibrational spectroscopic examination of Langmuir-Blodgett mono- and multilayer fatty acids by high-resolution electron energy loss spectroscopy, Langmuir 2 (1986) 543–548, https://doi.org/10.1021/la00071a002.

[52] J.J. Pireaux, P.A. Thiry, R. Caudano, P. Pfluger, Surface analysis of polyethylene and hexatriacontane by high resolution electron energy loss spectroscopy, J. Chem. Phys. 84 (1986) 6452–6457, https://doi.org/10.1063/1.450852.
[53] C.J. Powell, A. Jablonski, I.S. Tilinin, S. Tanuma, D.R. Penne, Surface sensitivity of Auger-electron spectroscopy and X-ray photoelectron spectroscopy, J. Electron Spectrosc. Relat. Phenom. 98–99 (1999) 1–15, https://doi.org/10.1016/S0368-2048(98)00271-0.
[54] M. Morscher, M. Corso, T. Greber, J. Osterwalder, Formation of single layer h-BN on Pd(111), Surf. Sci. 600 (2006) 3280–3284, https://doi.org/10.1016/j.susc.2006.06.016.
[55] E. Ćavar, R. Westerström, A. Mikkelsen, E. Lundgren, A.S. Vinogradov, M.L. Ng, A. B. Preobrajenski, A.A. Zakharov, N. Mårtensson, A single h-BN layer on Pt(111), Surf. Sci. 602 (2008) 1722–1726, https://doi.org/10.1016/j.susc.2008.03.008.
[56] A. Nagashima, N. Tejima, Y. Gamou, T. Kawai, C. Oshima, Electronic dispersion relations of monolayer hexagonal boron nitride formed on the Ni(111) surface, Phys. Rev. B 51 (1995) 4606, https://doi.org/10.1103/PhysRevB.51.4606.
[57] T. Aizawa, R. Souda, S. Otani, Y. Ishizawa, C. Oshima, Anomalous bond of monolayer graphite on transition-metal carbide surfaces, Phys. Rev. Lett. 64 (1990) 768, https://doi.org/10.1103/PhysRevLett.64.768.
[58] A.J. Van Bommel, J.E. Crombeen, A. Van Tooren, LEED and Auger electron observations of the SiC(0001) surface, Surf. Sci. 48 (1975) 463–472, https://doi.org/10.1016/0039-6028(75)90419-7.
[59] I. Forbeaux, J.M. Themlin, J.M. Debever, Heteroepitaxial graphite on 6H-SiC (0001): interface formation through conduction-band electronic structure, Phys. Rev. B 58 (1998) 16396, https://doi.org/10.1103/PhysRevB.58.16396.